Proceedings of ASME Turbo Expo 2014: Turbine Technical Conference and Exposition
GT2014
June 16-20, 2014, Dusseldorf, Germany

GT2014-25184

ON THE POTENTIAL OF A MULTI-FIDELITY G-POD BASED APPROACH FOR OPTIMIZATION & UNCERTAINTY QUANTIFICATION

David J.J. Toal
Astronautics, Aeronautics and Computational Engineering
Faculty of Engineering & the Environment
University of Southampton
Southampton, United Kingdom, SO17 1BJ
Email: djjt@soton.ac.uk

ABSTRACT

Traditional multi-fidelity surrogate models require that the output of the low fidelity model be reasonably well correlated with the high fidelity model and will only predict scalar responses. The following paper explores the potential of a novel multi-fidelity surrogate modelling scheme employing Gappy Proper Orthogonal Decomposition (G-POD) which is demonstrated to accurately predict the response of the entire computational domain thus improving optimization and uncertainty quantification performance over both traditional single and multi-fidelity surrogate modelling schemes.

NOMENCLATURE

- $\boldsymbol{C}$ Correlation matrix
- $\boldsymbol{f}$ Vector of fluctuations from the ensemble mean
- $\boldsymbol{F}$ Matrix of fluctuations from the ensemble mean
- k No. of POD snapshot vectors
- $\boldsymbol{m}$ Masking vector
- $\boldsymbol{s}$ POD snapshot vector
- $\bar{\boldsymbol{s}}$ POD ensemble mean
- $\boldsymbol{S}$ POD snapshot ensemble
- $\boldsymbol{u}$ Incomplete snapshot vector
- $\boldsymbol{V}$ Matrix of Eigenvectors
- $\boldsymbol{\alpha}$ Vector of POD modal coefficients
- $\boldsymbol{\beta}$ G-POD reconstruction model coefficients
- $\boldsymbol{\Lambda}$ Vector of Eigenvalues
- $\boldsymbol{\phi}$ Eigenfunctions
- $\boldsymbol{\Phi}$ Matrix of Eigenfunctions

INTRODUCTION

The majority of engineering design optimization workflows employ a simulation based on a discretized geometry followed by a series of post-processing operations to convert nodal or cell centred information into a number of key scalar values. These values are then used as either objectives or constraints by an optimization algorithm which, in the case of a costly simulation, may involve some form of surrogate model to reduce the number of simulations required. In some cases the overall cost of the optimization can be substantially reduced through the application of a multi-fidelity surrogate model, whereby data from high fidelity simulations is augmented by data from low fidelity simulations resulting in a more accurate model.

Figure 1(a) illustrates the classical example of the benefits of multi-fidelity surrogate modelling using an example recreated from Forrester et al. [1]. Here it can be observed that sampling an expensive function at four points and constructing a surrogate model through these points produces a relatively inaccurate response. However, Figure 1(a) illustrates that a much more accurate prediction of the expensive function can be made if the four expensive sample points are augmented by 11 additional sample points from a cheap function within a multi-fidelity surrogate model. In this case the resulting surrogate model is indistinguishable from the true function and predicts the global optimum almost exactly.

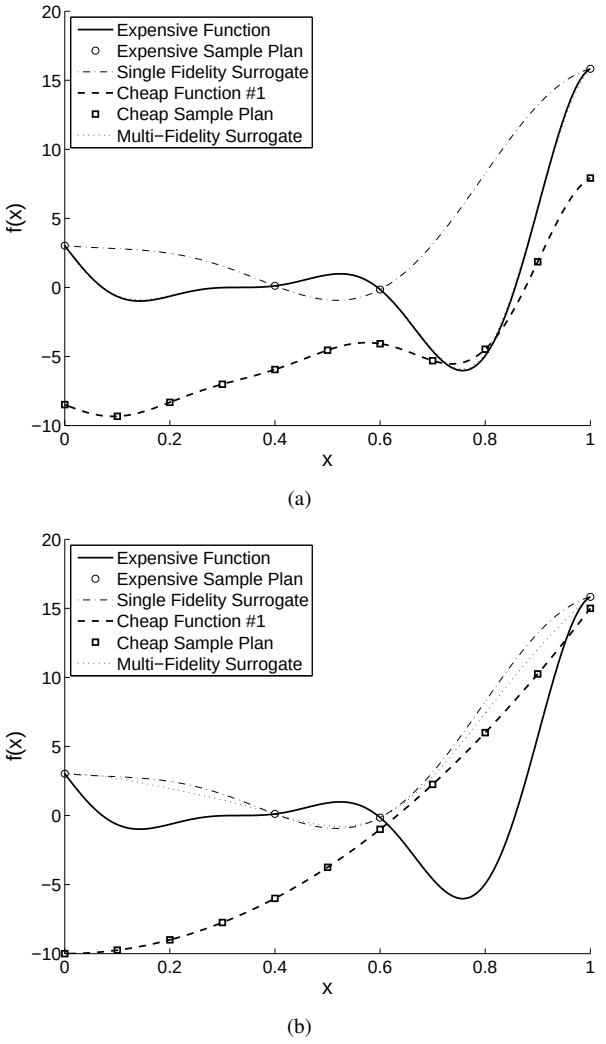

FIGURE 1. EXAMPLE MULTI-FIDELITY SURROGATE MODELS USING SIMILAR (a) & DISSIMILAR (b) LOW FIDELITY FUNCTIONS.

Figure 1(b), however, illustrates the potential pitfalls of blindly employing such a technique. In this case a surrogate model is constructed from the same four expensive sample points but the cheap sample points are taken from a different function, one which bears little resemblance to the expensive function. In this case the resulting multi-fidelity model is very similar to the single fidelity model, no benefit has been obtained from including the additional information. In cases where the cheap and expensive functions are poorly correlated the resulting multi-fidelity surrogate may actually be considerably less accurate than the single fidelity model.

In real world engineering design optimizations the application of traditional multi-fidelity surrogate modelling techniques, such as Co-Kriging [2], therefore requires there to be some level of underlying correlation between the high and low fidelity functions for the optimization to benefit. A surrogate based optimization of airfoil drag based on high fidelity RANS simulations, for example, would benefit little from being augmented with drag information from an inviscid panel code as there is no underlying correlation for a multi-fidelity surrogate to exploit. However, a surrogate model predicting lift coefficient would benefit as this output is much more closely correlated. This highlights a fundamental flaw of traditional multi-fidelity surrogate models, even though there is correlation in the results of these simulations at some level, for example the airfoils pressure profile, the requirement to post-process this data into scalar quantities of interest, as this is what traditional optimizers and surrogate models are based upon, prevents such correlations from being fully exploited.

The following paper explores the potential of a novel surrogate modelling and design optimization approach based on gappy proper orthogonal decomposition (G-POD) in which the G-POD is used to predict the nodal values of a high fidelity simulation using the nodal values of a low fidelity simulation. The reconstructed high fidelity simulation values can then be post-processed to determine the scalar quantities of interest. The presented approach is capable of accurately predicting the high fidelity simulation nodal data and therefore the high fidelity objective and constraints which can be either used directly by the optimization algorithm or used to provide additional data for a surrogate model. The applicability of this approach is demonstrated with respect to both the design optimization and uncertainty quantification of two engineering problems and compared to traditional surrogate modelling approaches.

We commence this paper by introducing both proper orthogonal decomposition (POD) and G-POD in terms of both their mathematics and previous applications within engineering and design. The proposed G-POD multi-fidelity design optimization framework is then presented in detail and contrasted to other similar strategies within the literature. The predictive capability of the presented approach is then demonstrated using an airfoil drag polar and a simple airfoil design problem. These problems are used to illustrate the performance advantages of the presented approach compared to conventional single and multi-fidelity surrogate modelling design optimizations strategies. Finally the performance of the proposed G-POD approach is demonstrated with respect to predicting the nodal variations of a gas turbine rotor model under a transient cycle in the presence of uncertainties in heat transfer coefficient.

POD & G-POD

Proper orthogonal decomposition (POD) has found many applications within the fields of computational fluid dynamics (CFD) [3, 4], reduced order modelling [5], design optimization [6–9] and surrogate modelling [10, 11]. POD aims to decompose

an ensemble of data snapshots into a set of orthogonal basis functions which are optimal in the sense that no other basis functions capture as much information in as few dimensions.

As per Sirovich's method of snapshots [12], POD begins by first defining a data ensemble $\boldsymbol{S}$ consisting of k snapshot vectors $\boldsymbol{s}$,

$$\boldsymbol{S} = [\boldsymbol{s}_1, \boldsymbol{s}_2, ..., \boldsymbol{s}_k]. \tag{1}$$

Once defined the data ensemble is decomposed into a mean $\bar{\boldsymbol{s}}$ and a matrix of fluctuations $\boldsymbol{F}$,

$$\boldsymbol{S} = \bar{\boldsymbol{s}} + \boldsymbol{F}, \tag{2}$$

where,

$$\bar{\boldsymbol{s}} = \frac{1}{k}\sum_{i=1}^{k} \boldsymbol{s}_i. \tag{3}$$

The orthogonal basis functions are then calculated by considering the solution to the following Eigenvalue problem,

$$\boldsymbol{CV} = \boldsymbol{\Lambda V}, \tag{4}$$

where $\boldsymbol{\Lambda}$ is a vector of Eigenvalues and $\boldsymbol{C}$ is the correlation matrix defined as, $\boldsymbol{C} = \boldsymbol{F}^T\boldsymbol{F}$. Given the matrix of Eigenvectors $\boldsymbol{V}$, the matrix of k Eigenfunctions can be calculated as,

$$\boldsymbol{\Phi} = \boldsymbol{FV}. \tag{5}$$

Using these Eigenfunctions, a corresponding vector of modal coefficients and the mean, each of the original snapshots can be exactly reconstructed,

$$\boldsymbol{s}_i = \bar{\boldsymbol{s}} + \boldsymbol{\Phi\alpha}_i. \tag{6}$$

POD is attractive because not all k basis functions are required to recreate each snapshot to a desired level of accuracy. Instead the cumulative percentage variation [13], based on the magnitude of the Eigenvalues can be used to select the first l most important basis functions. Equation 6 therefore becomes,

$$\boldsymbol{s}_i \approx \bar{\boldsymbol{s}} + \sum_{j=1}^{l} \boldsymbol{\alpha}_{i_j}\boldsymbol{\phi}_j. \tag{7}$$

With a set of basis functions calculated from an initial snapshot ensemble gappy proper orthogonal decomposition can be used to reconstruct any missing data from a new snapshot. This technique has been used in the past for the reconstruction of images from corrupted data [14], to map between design spaces of variable complexity [15], to predict aerodynamic flow fields [3,4] and even airfoil performance [16, 17].

Given a snapshot vector $\boldsymbol{u}$ with both known and unknown data, the first operation in reconstructing the missing data is to define a so called "mask" vector, $\boldsymbol{m}$ containing a Boolean indicator as to whether the information contained in the corresponding element of $\boldsymbol{u}$ is missing or not,

$$\boldsymbol{m}_i = 1 \quad \text{if} \quad \boldsymbol{u}_i \quad \text{is} \quad \text{known} \tag{8}$$

$$\boldsymbol{m}_i = 0 \quad \text{if} \quad \boldsymbol{u}_i \quad \text{is} \quad \text{unknown}, \tag{9}$$

where i here denotes the i^{th} data element in the vector $\boldsymbol{u}$. This indexing is extremely easy to implement with the help of Matlab's logical operators.

The aim of G-POD is to define a set of modal coefficients, $\boldsymbol{\beta}$, which best reconstruct the missing data based on a minimisation of the error between the known data and a POD reconstruction of that known data using those modal coefficients [16]. Once the index has been defined the mean (defined from the previous POD) is subtracted from the incomplete snapshot vector,

$$\boldsymbol{f} = \boldsymbol{u} - \bar{\boldsymbol{s}}, \tag{10}$$

with the missing values defined by the mask vector having been ignored. The modal coefficients are then calculated by solving the following set of linear equations,

$$(\boldsymbol{\Phi}^T\boldsymbol{\Phi})\boldsymbol{\beta} = \boldsymbol{\Phi}^T\boldsymbol{f}, \tag{11}$$

where only the l most important basis functions defined by the POD and only the data from these basis functions corresponding to known data in $\boldsymbol{u}$ is used.

The resulting set of modal coefficients, $\boldsymbol{\beta}$, can then be used along with the POD basis functions to recreate the missing data from the original snapshot vector, $\boldsymbol{u}$.

G-POD FOR MULTI-FIDELITY OPTIMISATION

Traditional surrogate modelling based design optimizations generally follow a similar process to that illustrated in Fig. 2. An initial design of experiments sampling plan is defined for the design variables of interest with computational simulations then performed at each of these design points. These simulations are

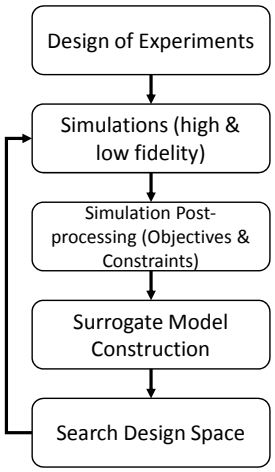

FIGURE 2. A TRADITIONAL OPTIMIZATION WORKFLOW.

then post-processed to obtain the necessary objective and constraint functions for the optimization. A surrogate model can then be constructed for each objective and constraint and used to perform a search of the design space, typically using an evolutionary algorithm. Any potentially good designs that have been identified by this search can then be evaluated using the computational simulation. Typically the process repeats until a stopping criterion has been reached or a predefined budget of simulations has been exhausted.

In the case of a multi-fidelity optimization, simulations are performed using a high and low fidelity computational model with objectives and constraints resulting from both models combined within a single multi-fidelity surrogate model [2]. Generally the low fidelity simulations are carried out over a much larger sampling plan than the high fidelity simulations. If well correlated this additional data helps to improve the accuracy of the multi-fidelity surrogate model and therefore helps to accelerate the optimization. Both single and multi-fidelity surrogate modelling based optimizations have been demonstrated to be very effective on a wide range of problems throughout the literature [18–22].

Taking inspiration from Willcox's [4] G-POD prediction of flow field data using pressure sensor information, the proposed G-POD based optimization methodology, illustrated in Fig. 3, takes a slightly different approach. As per a traditional surrogate based optimization, a design of experiments is defined and both low and high fidelity simulations are carried out at these points. However, unlike a more traditional multi-fidelity approach, both the low and high fidelity sampling plans are identical. Once the simulations have been carried out, information from the low and high fidelity computational domains for each design point is then combined within a snapshot ensemble and the POD performed.

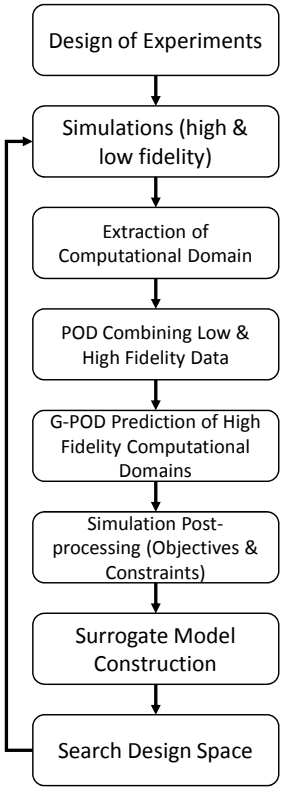

FIGURE 3. PROPOSED G-POD OPTIMIZATION WORKFLOW.

In this instance "computational domain" refers to nodal values throughout the simulation of interest, in the case of a computational fluid dynamics (CFD) simulation this may be nodal values of pressure or velocity while in the case of a finite element analysis (FEA) this may be nodal values of stress or displacement.

Additional low fidelity simulations can then be performed throughout the design space and, using the nodal information from these simulations as known data within a snapshot vector, the G-POD technique can be used to predict the unknown nodal quantities from the corresponding high fidelity computational domain. Given this prediction standard post-processing techniques can then be used to calculate the objectives or constraints of interest.

With a suitably cheap low fidelity simulation and post-processing process the evolutionary algorithm performing the design search could even directly employ the G-POD prediction to perform the search thereby removing the need for a traditional surrogate model to be used at all. Alternatively, if the expense of low fidelity simulation still prevents such a direct optimization being performed the G-POD predictions could be used to enhance more traditional surrogate models of the objectives and constraints. This additional information could be spread throughout the design space in a similar manner to a multi-fidelity sur-

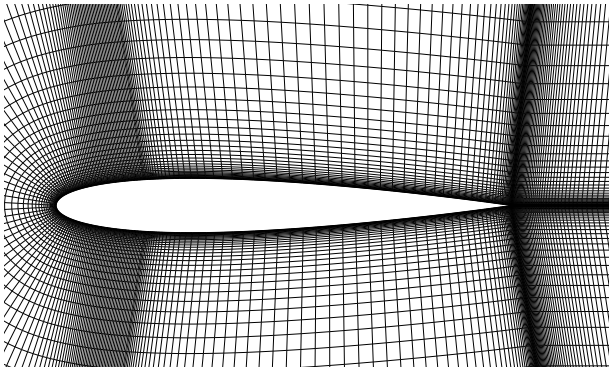

FIGURE 4. NACA 0012 CFD MESH.

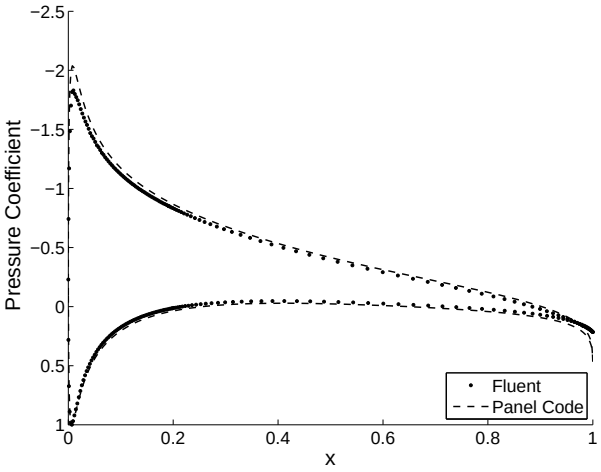

FIGURE 5. NACA 0012 PRESSURE PREDICTIONS.

rogate model or close to the original high fidelity sampling plan resulting in a pseudo-gradient enhanced surrogate.

The proposed approach has a number of similarities with other G-POD based design methods presented within the literature. Bui-Thanh and Willcox [16], for example, used G-POD to perform airfoil inverse design. Using a snapshot ensemble consisting of airfoil geometry and pressure distributions the authors used G-POD to calculate the airfoil geometry given a desired pressure distribution. In the approach presented here, however, no explicit geometry information is provided when the snapshots are defined, instead the process operates purely on the results of the simulation. Bui-Thanh and Willcox's approach could be modified for direct design by providing the airfoil geometry as the known data and using G-POD to predict the flow field although the technique may require further modification to predict flow fields for conditions where the geometry does not change, for example, as airfoil angle of attack varies.

LOW SPEED AIRFOIL DRAG POLAR PREDICTION

To better illustrate the presented multi-fidelity G-POD approach consider now its application to the prediction of the drag polar of the NACA 0012 airfoil. The airfoil will be simulated using both the commercial CFD package, ANSYS Fluent and a simple inviscid panel code [23].

The Fluent simulation employs a structured mesh with a CH topology generated using ANSYS ICEM 14.0. The mesh itself consists of approximately 32,000 elements and is illustrated in Fig. 4. Flow around the airfoil is modelled in Fluent using a pressure farfield boundary condition with the specified Mach number and with the x and y velocity components defined according to the angle of attack. The density of air is defined using the ideal gas law while the fluid viscosity is defined using Sutherland's law. The simulation also employs the Spalart-Allmaras turbulence model. Each airfoil simulation is run using a first order scheme for 500 iterations after which the simulation switches to a second order scheme for a further 3500 iterations. Although perhaps a little excessive this ensures that the drag and lift coefficients have converged acceptably for all angles of attack and for different airfoil designs. A single Fluent simulation of the airfoil takes approximately three minutes using a standard desktop computer. In the following example the NACA0012 airfoil is simulated at Mach 0.1 between $\pm 5°$angle of attack. The lower fidelity panel code is implemented in Matlab and employs a total of 200 panels (100 on each surface) around the airfoil geometry. A single simulation of the NACA 0012 using this code takes approximately one second to perform.

The Fluent simulation compares well to the experimental data from Abbott and Doenhoff [24] with the simulation predicting a drag coefficient of 9.73×10^{-3} at $0°$ angle of attack, 0.7% less than experimental result of 9.8×10^{-3}. Although the panel code cannot predict the drag coefficient of the airfoil very accurately it does produce a relatively accurate prediction of the airfoil's pressure coefficient which allows the simulation to accurately predict the lift generated by the airfoil. The Fluent and panel simulations predict lift coefficients of 0.542 and 0.596 respectively for the NACA 0012 at 5°which is close to experimental result of 0.550. Figure 5 illustrates that apart from a slight under prediction in the suction side pressure at the leading edge and an over prediction at the trailing edge there is very little difference in pressure distributions resulting from the two simulations at 5°.

To create a G-POD multi-fidelity prediction of the drag polar of the NACA 0012 between -5°and +5°angle of attack we first define a sampling plan defining the initial Fluent and panel code simulations. In this case three sample points have been defined at angles of attack of -5°, 0°and +5°. Having performed the Fluent simulations the velocities, pressures, temperatures and turbulent viscosity values at every single node are extracted along with the

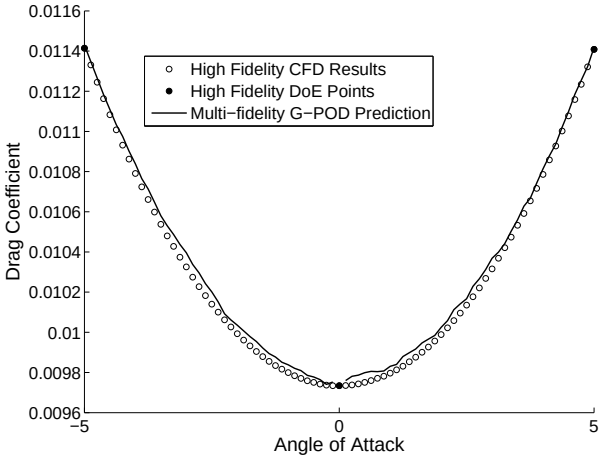

FIGURE 6. G-POD DRAG POLAR PREDICTION.

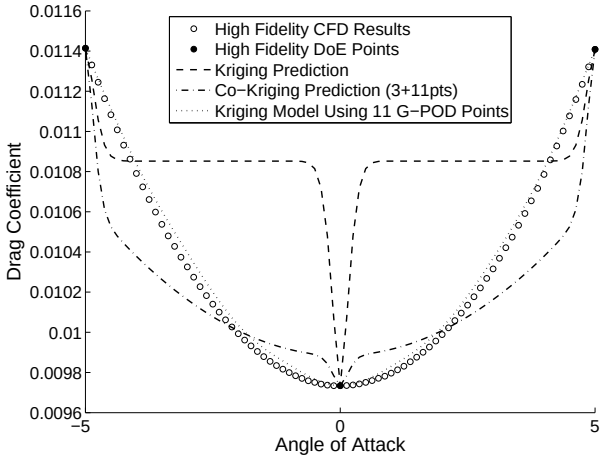

FIGURE 7. SURROGATE DRAG POLAR PREDICTIONS.

pressure distribution from the panel code and used to define three snapshot vectors. A POD is then performed using this ensemble with the basis functions and pressure distributions at intermediate angles of attack coming from the panel code used in a G-POD to predict the nodal properties of the corresponding Fluent simulation. These quantities are then post-processed to calculate the drag coefficient.

It should be noted that the cost of the proposed G-POD process, including both the initial POD and gappy reconstruction, is negligible compared to the cost of a single high fidelity CFD simulation. Using this approach the reconstruction of the above nodal quantities is almost instantaneous. The cost of the nodal reconstruction is much more dependent on the expense of the underlying low fidelity simulation used to provide the known data for the gappy reconstruction. In this case the 2D panel code runs in under a second but for larger more complex 3D cases this computation time may increase considerably.

Figure 6 illustrates the resulting mulit-fidelity G-POD prediction of the drag polar of the NACA 0012 as compared to 81, high fidelity, Fluent simulations equally distributed between $\pm 5°$. Using G-POD in this manner the prediction of drag appears to be very accurate with a maximum absolute error (MAE) of 7.05×10^{-5}, a root mean square error (RMSE) of 3.92×10^{-5} and an r^2 correlation of 0.9996.

As a comparison to the G-POD drag polar prediction, consider now the performance of two popular surrogate modelling techniques, Kriging [25] and Co-Kriging [2]. Figure 7 presents the results of surrogate models constructed using these methods. In the case of both of these models the same three high fidelity sampling points that were employed in the creation of the G-POD model are used. In the case of the Co-Kriging model, a multi-fidelity surrogate modelling technique, the drag values at these three points are augmented by panel code drag predictions from an additional 11 points equally spaced between $\pm 5°$.

Figure 7 clearly illustrates that the Kriging model does not have enough information to accurately represent the drag polar. This results in an overestimation of the Kriging hyperparameter defining the rate of correlation decrease leading to a Kriging model with sudden jumps from a constant mean to the sample point value. The Co-Kriging model produces a slightly better prediction of the drag polar but is mislead by the extremely poor predictions of drag from the panel code used to construct the model.

As noted previously the G-POD prediction could be used directly in any subsequent search of the design space if the combined cost of both the low fidelity model and any necessary post-processing are comparable to that of a surrogate model. Figure 7 also illustrates an alternative approach if this is not the case. Here a Kriging model has been constructed using drag values obtained from 11 equally spaced G-POD predictions from Fig. 6. This surrogate model now has the accuracy of the G-POD model while retaining the evaluation speed of a standard Kriging model. Although 11 G-POD simulations have been used here, the drag values from the three original Fluent simulations could also have been retained and augmented with eight G-POD drag predictions in between them. As G-POD recreates the original snapshots exactly the drag prediction at these points is almost identical to that from the original simulation.

HIGH ANGLE OF ATTACK DRAG POLAR PREDICTION

While the previous section illustrated the predictive capabilities of the G-POD approach with regard to a drag polar, the angles of attack used could be considered relatively moderate. To further assess the approach consider now the application of the G-POD approach to the prediction of the drag polar of the NACA

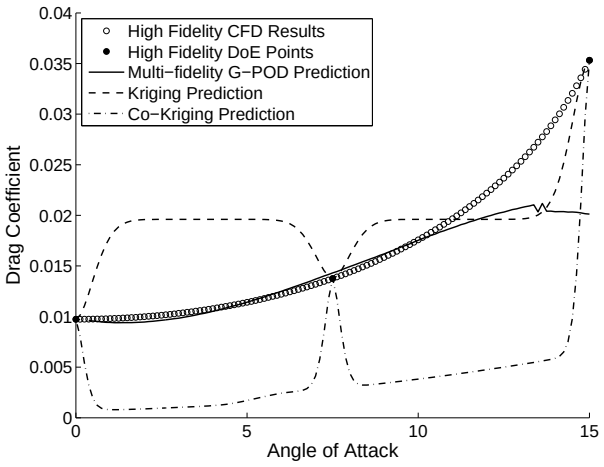

FIGURE 8. HIGH ANGLE OF ATTACK DRAG POLAR PREDICTIONS.

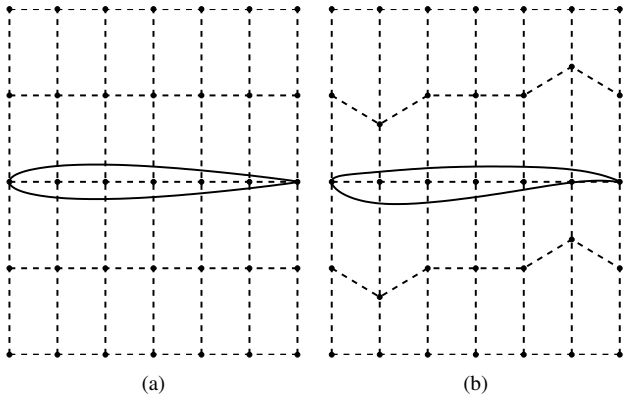

FIGURE 9. FFD CONTROL LATTICES.

0012 airfoil from 0° to 15° angle of attack. As the angle of attack approaches 15° a separation bubble begins to develop on the trailing edge of the airfoil. This should make it much harder for the multi-fidelity G-POD approach to accurately predict the nodal quantities of the high fidelity CFD simulation as the snapshots employed do not adequately capture the evolution of this particular flow feature.

As with the drag polar example in the previous section a total of three high fidelity simulations will be performed, this time at 0°, 7.5° and 15°angle of attack. Once again the pressure distribution resulting from the panel code simulation will be used along with G-POD to predict the nodal quantities for intermediate angles of attack. Figure 8 illustrates the G-POD prediction along with the corresponding Kriging and Co-Kriging predictions.

Both the Kriging and Co-Kriging predictors offer a relatively poor representation of the drag polar over this range of angles of attack. The Kriging prediction results in an r^2 correlation of 0.6612, a RMSE of 6.04×10^{-3} and a MAE of 9.6×10^{-3}. Unlike the previous case, where the Co-Kriging prediction was slightly more accurate than the Kriging prediction, in this case the accuracy is substantially reduced with the resulting model exhibiting an r^2 correlation of 0.640, a RMSE of 1.31×10^{-2} and a MAE of 2.43×10^{-2}. Over the majority of the drag polar, the multi-fidelity G-POD approach is much more accurate than both of these traditional surrogate modelling approaches. From 0° to 15°, G-POD predicts the drag polar with an r^2 correlation of 0.915, a RMSE of 3.83×10^{-3} and a MAE of 1.52×10^{-2}. Figure 8 also illustrates that the G-POD prediction is much more accurate below an angle of attack of 10°, in this region the model predicts the drag polar with an r^2 correlation of 0.995, a RMSE of 3.83×10^{-4} and a MAE of 5.55×10^{-4}.

In conclusion, this example illustrates that while the approach works well for low to moderate angles of attack as soon as effects such as separation start to come into play the multi-fidelity G-POD based approach begins to loose accuracy. This reduction in accuracy may, however, be countered through an increase in the number of high fidelity snapshots in such regions or a reduction in the bounds of the design space that the G-POD approach is used to represent. Never-the-less over the 0-15°domain the G-POD approach offers a considerable improvement over the accuracy of Kriging and Co-Kriging for an equivalent cost.

TWO VARIABLE DESIGN SPACE PREDICTION

While the accurate prediction of an airfoil's drag polar with a small number of expensive simulations is useful in itself for robust and multi-point design optimizations, G-POD is operating only in one dimension. Let us now investigate the proposed G-POD approach in the context of a design optimization, in this case the optimization of the NACA 0012 airfoil for minimum drag.

As before the airfoil is simulated using both high and low fidelity CFD but this time at a fixed angle of attack of 2°. A freeform deformation (FFD) based parameterization is used to morph the nodes defining the computational mesh and panel coordinates. In this case the airfoil geometry is enclosed in a lattice of 35 FFD control points [26], illustrated in Fig. 9(a), where the control points on the second and fourth horizontal line are permitted to move vertically by $\pm 1\%$ of the airfoils chord. Figure 9(b) illustrates the geometry resulting from perturbations to four FFD control points resulting in a reduction in camber close to the leading edge and an increase in camber at the trailing edge.

Morphing the computational domain using FFD has been used with great success in the literature to perform aerodynamic design optimizations [27–29] as it reduces the amount of noise in the design space caused by variations in mesh topology. The consistent node numbering and connectivity from one design to another also simplifies the G-POD strategy presented here by re-

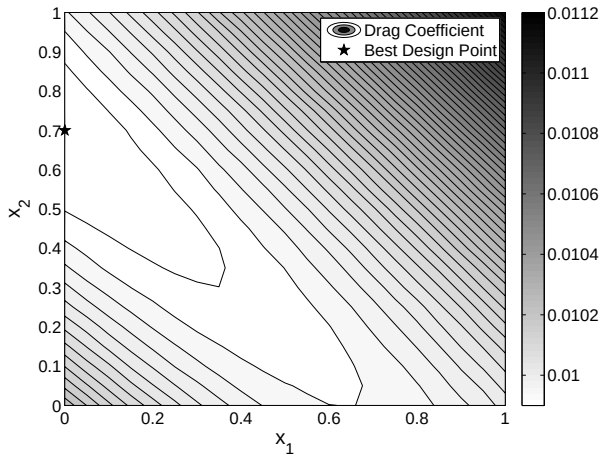

FIGURE 10. TWO VARIABLE AIRFOIL DESIGN SPACE.

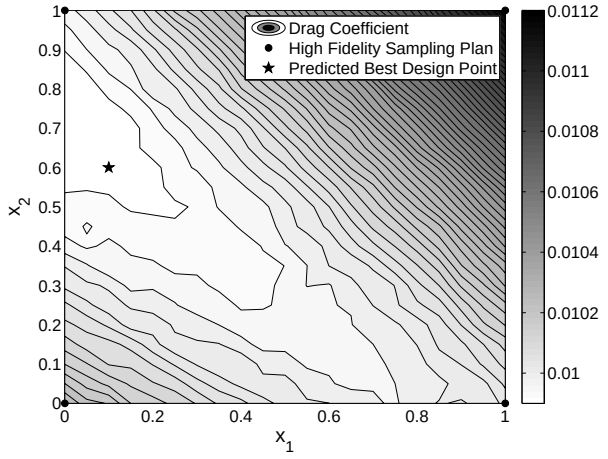

FIGURE 11. TWO VARIABLE G-POD PREDICTION.

moving the need to map flow field information between meshes.

Consider now a two variable optimization of the NACA 0012 where only the two FFD control points at the trailing edge of the airfoil are permitted to vary. Figure 10 illustrates the resulting design space created from a 21×21 grid of high fidelity CFD simulations. It should also be noted that the movement of the control points has been normalized to between zero and one and that the star in Fig. 10 indicates the design with the minimum drag from those considered on the 21×21 grid.

In order to predict the design space using multi-fidelity G-POD a four point sampling plan is used with one point at each corner of the design space (see Fig. 11). A POD is then performed of the high fidelity CFD flow field and the pressure distribution from the low fidelity CFD for the corresponding designs. Predictions of the high fidelity flow field are then made

TABLE 1. TWO VARIABLE DESIGN SPACE PREDICTION ACCURACY.

Method	r^2	RMSE	MAE
G-POD	0.998	4.09×10^{-5}	8.56×10^{-5}
Kriging	0.281	3.27×10^{-4}	6.24×10^{-4}
Co-Kriging	0.453	2.22×10^{-4}	5.88×10^{-4}
Kriging & 21 G-POD	0.998	4.24×10^{-5}	8.48×10^{-5}
Kriging & 8 G-POD	0.982	1.35×10^{-4}	1.99×10^{-4}

at unknown points using the pressure distribution from the low fidelity simulation at that point and G-POD.

Figure 11 illustrates the multi-fidelity G-POD prediction of the two variable airfoil design space using the same 21×21 grid of points used in the construction of Fig. 10. Whilst there is some degree of noise in the prediction, the G-POD approach does accurately represent the variation in drag throughout the design space. This is confirmed statistically in Tab. 1, where the G-POD prediction of drag correlates extremely well with the true values, $r^2 = 0.998$, and the maximum absolute error (MAE) and root mean square error (RMSE) are very low at 8.56×10^{-5} and 4.09×10^{-5} respectively. Although the G-POD prediction is generally accurate the additional noise in the response has resulted in a slight inaccuracy in the prediction of the optimal design.

Consider now Kriging and Co-Kriging predictions of the same design space using the same four point sampling plan. Figure 12(a) illustrates the resulting Kriging model which, as with the drag polar does not contain enough information to produce a reasonable surrogate model. Once again the rate of change of correlation resulting from the hyperparameter optimization is too large producing a model with a rapid change in response away from each sample point towards the mean. The Co-Kriging model, Fig. 12(b), which contains the four high fidelity sample points and an additional 25 low fidelity sample points, is slightly more accurate than the Kriging model (according to the statistics in Tab. 1) but performs no better at predicting where the optimum design is. Both the Kriging and Co-Kriging models perform considerably worse than the G-POD approach. The r^2 correlation of both responses are less than half that of G-POD while the RMSE and MAE are both an order of magnitude greater.

As per the drag polar prediction, let us now consider using the results from a number of G-POD predictions to augment the Kriging model of Fig. 12(a). Figure 12(c) illustrates the prediction of a Kriging model constructed from four high fidelity CFD drag coefficients and G-POD predicted drag coefficients at the same low fidelity points used to construct the Co-Kriging model of Fig. 12(b). In this case there is a substantial improvement in the accuracy of the model all be it at a marginal increase in total

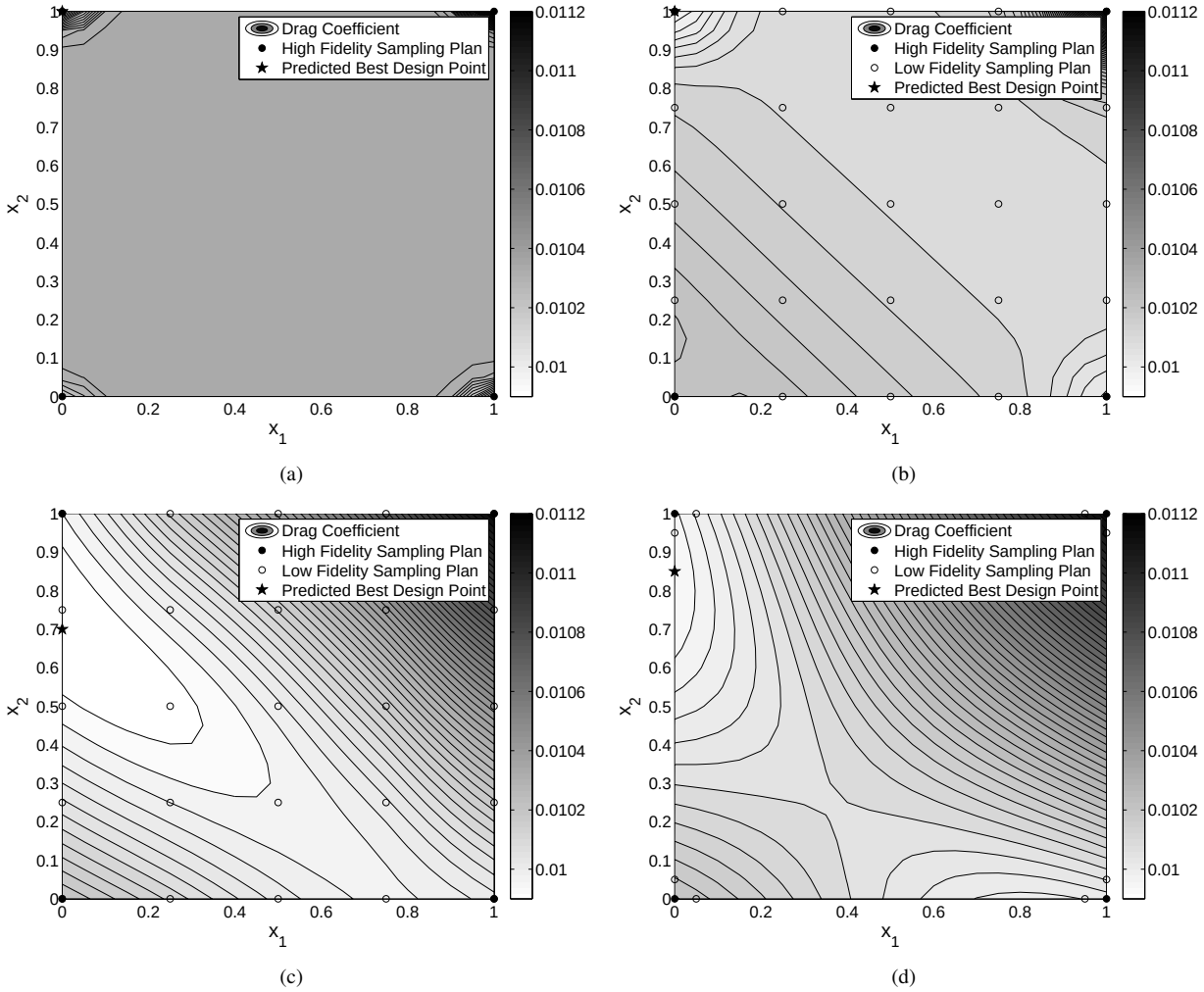

FIGURE 12. TWO VARIABLE KRIGING (a), CO-KRIGING (b) & KRIGING PREDICTIONS USING G-POD DERIVED DATA THROUGHOUT THE DESIGN SPACE (c) & AT POINTS PERTURBED FROM THE HIGH FIDELITY SAMPLE POINTS (d).

computational cost over that to create the Co-Kriging model due to the cost of post-processing the high fidelity flow field prediction. As indicated by the statistics in Tab. 1 this model is as accurate as the pure G-POD prediction but with the noise removed from the response due to the smoothing effect of the surrogate model. In this case the prediction of the optimum exactly corresponds with that of the true design space, Fig. 10.

As previously noted as well as providing points to populate the rest of the design space with, G-POD predictions could also be used to predict points close to existing high fidelity points thereby producing a pseudo gradient enhanced surrogate model. Figure 12(d) illustrates such a model where the four high fidelity CFD points have each been augmented by two additional G-POD predictions a short distance away in the direction of each design variable. According to the statistics presented in Tab. 1 the resulting surrogate model is less accurate in terms of RMSE and MAE than both the G-POD prediction and the Kriging & G-POD prediction but is still extremely well correlated with the true design space. The prediction of the global optimum is also quite close to the true optimum indicated in Figures 10 and 12(c).

LOW SPEED AIRFOIL OPTIMIZATION

With initial surrogate models of the two variable design space defined let us now consider the application of these models within a design optimization. Recalling the optimization processes outlined in Figures 2 and 3 we take the standard single and multi-fidelity models and search them using an evolutionary algorithm to locate the optimum design. In this case the genetic algorithm provided by Forrester et al. [20] is used with a popula-

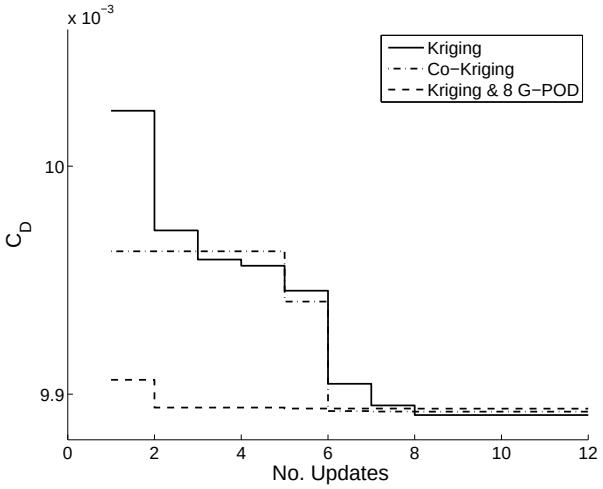

FIGURE 13. TWO VARIABLE OPTIMIZATION HISTORIES.

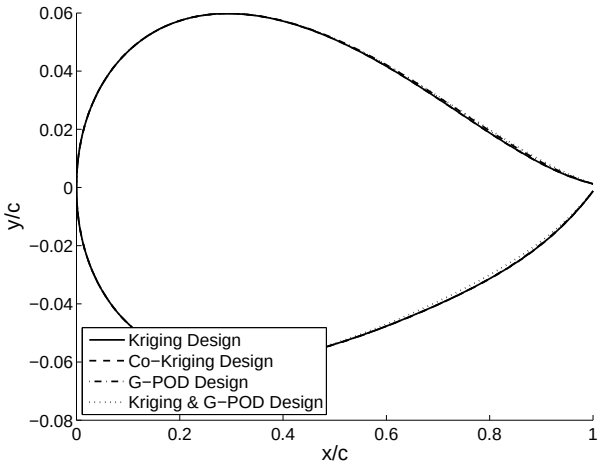

FIGURE 14. COMPARISON OF AIRFOIL DESIGNS RESULTING FROM EACH OPTIMIZATION.

tion size of 50 and run for 100 generations. This design point is then evaluated using the high fidelity CFD code and the resulting drag used to update the surrogate model. The model is searched again and the process repeats for, in this case, a total of 12 times.

Figure 13 illustrates the drag values found over the course of three optimizations. The Kriging optimization, denoted by the solid line, illustrates the history of an optimization commenced from the initial surrogate model illustrated in Figures 12(a). The Co-Kriging optimization, denoted by the dash-dot line, illustrates the history of an optimization commenced from the initial surrogate model illustrated in Fig. 12(b). Despite the poor initial representations of the design space both of these models eventually locate the optimum design. The improved accuracy of the Co-Kriging model gives it a slightly better optimization performance and allows it to find the optimum two updates before the Kriging based optimization.

Figure 13 also illustrates the performance of a Kriging & 8 G-POD based optimization. Represented by the dashed line in this plot, this strategy commences from the surrogate model illustrated in Fig. 12(d). The optimization history for this strategy presented in Fig. 13 demonstrates a considerable acceleration in convergence towards an optimum over the other two strategies. In fact within two updates the optimization has converged to the optimum design.

Not presented in Fig. 13 is the convergence history for an optimization commencing from the Kriging & 21 G-POD model illustrated in Fig. 12(c). As noted previously, this surrogate model exactly predicts the location of the global optimum. The first update simulation would therefore fall on the exact global optimum.

It should also be noted that the slight differences in the final optimal drag values in Fig. 13 are due to a constraint within the search of the design space preventing two updates being too close together. Update points are prevented from being within 5×10^{-3} of any previous sample point. If the genetic algorithm results in a point within this range then a random perturbation is applied to the coordinates of the update point to move it away from the previous point. This process aims to prevent ill-conditioning in the correlation matrices used to construct the surrogate models and prevents the optimizations from stalling. Both figures 12(a) and 12(b) illustrate that the Kriging and Co-Kriging models suggest that the high fidelity sample point in the top left corner of the design space is the optimum. Without a perturbation to this predicted optimum from the previously sampled point the optimization would stall and produce no further improvement. It should be noted, however, that other updating schemes such as expected improvement [30] could also be used to ensure that updates do not fall on points already evaluated. Figure 14 illustrates the final airfoil designs. Each of the optimizations have resulted in broadly the same modifications to the baseline airfoil with only slight differences in the final designs due to the above constraint on the placement of update points.

UNCERTAINTY QUANTIFICATION OF A 2D ROTOR

The drag polar prediction and two variable aerodynamic design optimization have demonstrated the capabilities of the presented multi-fidelity G-POD approach with respect to fluid dynamics simulations. Let us now consider the application of this approach to a mechanical case study, specifically the prediction of uncertainties in a gas turbine engine rotor.

Figure 15 illustrates a simplified geometric model of the rotors in a two shaft gas turbine engine. Consisting of a three stage low pressure (LP) compressor, an eight stage high pressure (HP)

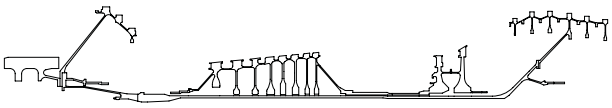

FIGURE 15. 2D GAS TURBINE ROTOR GEOMETRY.

compressor, a two stage HP turbine and a six stage LP turbine this model was created as part of the Collaborative and Robust Engineering using Simulation Capability Enabling Next Design Optimization (CRESCENDO) project to demonstrate the feasibility of whole engine design optimization. Although a 3D model of the static engine components exists here we shall investigate the use of G-POD using only the rotor model.

The rotor undergoes a transient thermo-mechanical simulation over a so called "square cycle" using the proprietary Rolls-Royce finite element package, SC03 [31, 32]. The rotor model consists of a total of 3494, second order, six node triangular elements with the cycle comprising of conditions at idle followed by an acceleration to max take-off, a deceleration to idle and a final acceleration to cruise. Thermal boundary conditions have been applied to each of the model's faces to represent convective heat transfer and radiation. Pressures, temperatures, heat transfer coefficients and flow directions have been specified for both oil and air for each of the cycle conditions. Given the model's 2D nature and relatively small number of degrees of freedom a single analysis can be performed on a desktop computer in under 5 minutes.

Within gas turbine design it is common to have to calculate the impact of uncertainties in heat transfer coefficients (HTCs) on temperatures and displacements. Consider now, therefore, using multi-fidelity G-POD to calculate the variation in displacements and temperatures in the above rotor model if the HTCs in the cavities of the HP compressor, HP turbine and LP turbine are permitted to simultaneously vary by $\pm 10\%$.

Unlike the previous aerodynamic examples the same simulation setup will be used to provide both the low and high fidelity simulation data. The low fidelity simulation will be a truncation of the high fidelity simulation with only the first 100 of the 156 time steps analysed. This is analogous to the work of Forrester et al. [33] who performed multi-fidelity design optimization using a mixture of fully and partially converged CFD simulations. The G-POD process will therefore begin with a series of complete simulations carried out over the range of HTC scaling parameters with data from cheaper simulations over a portion of the cycle used in a G-POD to predict the response of the rotor over the remaining cycle. The completed data sets can then be used to calculate the variation in temperature and displacement for every single node in the model for the given range in HTC.

This case study therefore illustrates a considerable advantage of the G-POD approach over traditional surrogate modelling approaches. The scalar nature of such surrogates prevents them

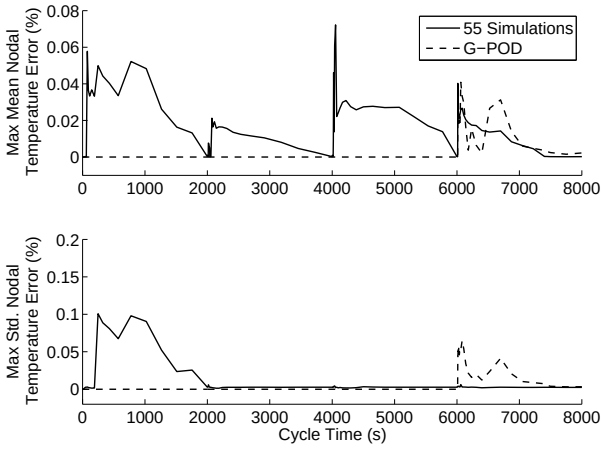

FIGURE 16. NODAL TEMPERATURE PREDICTION ERRORS.

from predicting the variance across the entire model. The multi-fidelity G-POD strategy proposed here cannot, therefore, be directly compared to a traditional surrogate modelling strategy as was the case in the previous examples. Instead it shall be compared to an equivalent costing number of full fidelity simulations.

After a short study it was determined that 81 rotor simulations at equally spaced values of $\pm 10\%$ HTC gave an acceptably converged mean and standard deviation. This will therefore be considered as the standard to which the subsequent prediction methods shall be compared.

To summarize the G-POD strategy consists of 9 full fidelity simulations in which the rotor has been analysed over the complete cycle and 72 low fidelity simulations in which the rotor is simulated for only the first 6000 seconds, i.e., up until the acceleration from idle to cruise conditions. As noted above each of these truncated simulations runs for 100 time steps as opposed to 156 for the complete simulation which means that each simulation costs 64% of the equivalent full fidelity simulation. Including the 9 full fidelity simulations, the G-POD strategy is therefore 68% of the total cost of carrying out 81 complete rotor simulations. We therefore compare the G-POD strategy, not only to the results of the 81 simulation prediction but also to a 55 simulation prediction of equivalent cost to the G-POD approach.

Figure 16 illustrates the maximum error in the calculation of mean and standard deviation of all of the 9142 nodes within the rotor model taken as a percentage of the maximum nodal temperature at each time step. Similarly Figures 17 and 18 illustrate the maximum error in the calculation of nodal mean and standard deviation for both x and y displacements taken as a percentage of the maximum nodal value at each time step. In all three plots the errors are taken relative to the 81 simulation calculation with the 55 full fidelity simulation prediction represented by the solid line and the G-POD prediction represented by the dashed line.

As the G-POD strategy produces the same results as the 81

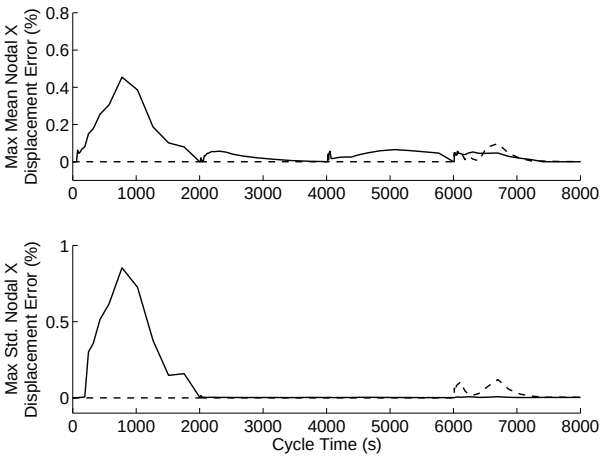

FIGURE 17. NODAL X DISPLACEMENT PREDICTION ERRORS.

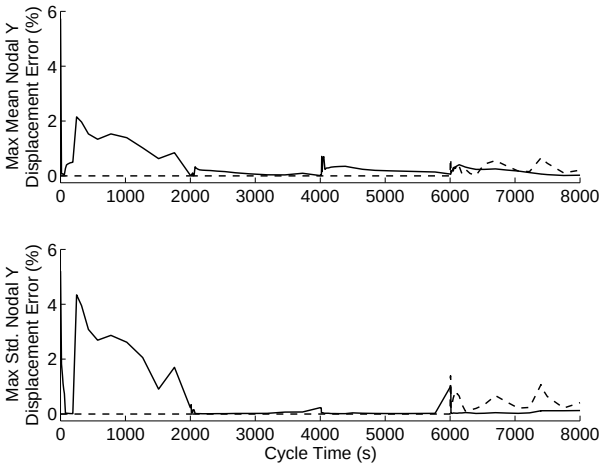

FIGURE 18. NODAL Y DISPLACEMENT PREDICTION ERRORS.

simulations over the first 6000 seconds of the cycle there is zero error in the calculations of mean and standard deviation for any node for either temperatures or displacements. The 55 simulation case, however, exhibits some quite large errors in this region, in particular over the first 2000 seconds where the simulation accelerates the rotor from idle to take-off conditions. The maximum error in the y displacement standard deviation, for example, is over 4% of the maximum standard deviation of the target 81 simulation case.

Between 6000 and 8000 seconds, however, the accuracy of the G-POD predictions of the nodal mean and standard deviations are more mixed. For some time steps the prediction is more accurate than the results of the equivalent costing 55 simulation case and in some cases the prediction is less accurate. Over the course of the cycle, however, the maximum error in the G-POD prediction in the final 2000 seconds is considerably lower than the maximum error in the 55 simulation prediction.

G-POD in this instance has reduced the cost of the uncertainty quantification of a gas turbine rotor by over 30% and produced more accurate results over the course of the cycle, no error in either the nodal mean or standard deviation is greater than 1% compared to the equivalent costing number of full fidelity simulations.

CONCLUSIONS

The current paper has explored the potential of a novel multi-fidelity G-POD strategy for surrogate modelling, design optimization and uncertainty quantification. Unlike traditional surrogate modelling strategies the proposed G-POD approach operates at the level of the nodal values within the computational domain prior to any form of post-processing. By using nodal data from low fidelity simulations a G-POD is used to predict nodal data within the equivalent high fidelity simulation which can then be post-processed as normal and employed directly within an optimization or used to augment a surrogate model.

The presented approach has been demonstrated to produce more accurate predictions of the drag polar of an airfoil and a two variable aerodynamic design space than equivalent costing Kriging and Co-Kriging models. The improvement in accuracy of the variation in drag throughout the airfoil design space was demonstrated to offer a considerable improvement in optimization performance. The approach has also been demonstrated to be competitive at reducing the cost of predicting the nodal uncertainties within a thermo-mechanical gas turbine rotor model.

Whilst this approach clearly has a great deal of potential to reduce computational effort within optimizations and improve surrogate model predictions, there remain a number of issues which still remain to be investigated. The current paper applied the G-POD approach to test cases with a relatively small number of dimensions. The applicability of this approach at higher dimensions and the definition of an appropriate sampling plan for this technique therefore remain to be investigated. Similarly the applicability of the technique to other more complex design problems employing three dimensional simulations also requires investigation. Also not considered within this paper is the re-evaluation of the POD basis functions as further high fidelity simulations are performed as an optimization progresses which, on higher dimensional problems may act to improve the accuracy of the prediction throughout the design space. Finally, further investigations into the application of this methodology to the prediction of transient responses need to be performed to determine appropriate limits for the application of this technique.

ACKNOWLEDGMENT

The support of Rolls-Royce and ANSYS in carrying out this work is greatly acknowledged.

REFERENCES

[1] Forrester, A., Sóbester, A., and Keane, A., 2007. "Multi-fidelity optimization via surrogate modelling". *Proceedings of the Royal Society A,* ***463***(2088), pp. 3251–3269.

[2] Kennedy, M., and O'Hagan, A., 2000. "Predicting the output from a complex computer code when fast approximations are available". *Biometrika,* ***87***(1), pp. 1–13.

[3] Venturi, D., and Karniadakis, G., 2004. "Gappy data and reconstruction procedures for flow past a cylinder". *Journal of Fluid Mechanics,* ***519***, pp. 315–336.

[4] Willcox, K., 2006. "Unsteady flow sensing and estimation via the gappy proper orthogonal decomposition". *Computers & Fluids,* ***35***, pp. 208–226.

[5] Lucia, D., and Beran, S., 2004. "Reduced-order model development using proper orthogonal decomposition and volterra theory". *AIAA Journal,* ***42***(6), pp. 1181–1190.

[6] LeGresley, P., and Alonso, J., 2000. "Airfoil design optimization using reduced order models based on proper orthogonal decomposition". In Fluids 2000 Conference and Exhibit.

[7] Li, G., Li, M., Azarm, S., Rambo, J., and Joshi, Y., 2007. "Optimizing thermal design of data centre cabinets with a new multi-objective genetic algorithm". *Distributed and Parallel Databases,* ***21***(2-3), pp. 167–192.

[8] My-Ha, D., Lim, K., Khoo, B., and Willcox, K., 2007. "Real-time optimisation using proper orthogonal decomposition: Free surface prediction due to underwater bubble dynamics". *Computers & Fluids,* ***36***(3), pp. 499–512.

[9] Toal, D., Bressloff, N., Keane, A., and Holden, C., 2011. "The development of a hybridized particle swarm for kriging hyperparameter tuning". *Engineering Optimization (Accepted for Publication)*.

[10] Xiao, M., Breitkopf, P., Coelho, R., Knopf-Lenoir, C., Sidorkiewicz, M., and Villon, P., 2010. "Model reduction by cpod and kriging: Application to the shape optimization of an intake port". *Structural and Multidisciplinary Optimization,* ***41***(4), pp. 555–574.

[11] Toal, D., and Keane, A., 2011. "Non-stationary kriging prediction of the performance of turbomachinery components". In European Turbomachinery Conference, Istanbul, Turkey, March $21^{st} - 25^{th}$.

[12] Sirovich, L., 1987. "Turbulence and dynamics of coherent structures part 1: Coherent structures". *Quarterly of Applied Mathematics,* ***45***(3), pp. 561–571.

[13] Jolliffe, I., 2002. *Principle Component Analysis*. Springer.

[14] Everson, R., and Sirovich, L., 1995. "Karhunen-loeve procedure for gappy data". *Journal of the Optical Society of America,* ***12***(8), pp. 1657–1664.

[15] Robinson, T., Willcox, K., Eldred, M., and Haimes, R., 2006. "Multifidelity optimization for variable-complexity design". In 11th AIAA/ISSMO Multidisciplinary Analysis and Optimization Conference, Portsmouth, Virginia.

[16] Bui-Thanh, T., and Willcox, K., 2004. "Aerodynamic data reconstruction and inverse design using proper orthogonal decomposition". *AIAA Journal,* ***42***(8), pp. 1505–1516.

[17] Duan, Y., Cai, J., and Li, Y., 2012. "Gappy proper orthogonal decomposition-based two-step optimization for airfoil design". *AIAA Journal,* ***50***(4), pp. 968–971.

[18] Queipo, N., Haftka, R., Shyy, W., Goel, T., Vaidyanathan, R., and Tucker, P., 2005. "Surrogate-based analysis and optimization". *Progress in Aerospace Sciences,* ***41***, pp. 1–28.

[19] Wang, G., and Shan, S., 2007. "Review of metamodeling techniques in support of engineering design optimization". *ASME Journal of Mechanical Design,* ***129***, pp. 370–380.

[20] Forrester, A., Sóbester, A., and Keane, A., 2008. *Engineering Design via Surrogate Modelling*. Wiley-Blackwell.

[21] Brooks, C., Forrester, A., Keane, A., and Shahpar, S., 2011. "Multi-fidelity design optimisation of a transonic compressor rotor". In 9th European Turbomachinery Conference, Istanbul, Turkey, 21st-25th March.

[22] Toal, D., and Keane, A., 2011. "Efficient multi-point aerodynamic design optimization via co-kriging". *Journal of Aircraft,* ***48***(5), pp. 1685–1695.

[23] Katz, J., and Plotkin, A., 2008. *Low-Speed Aerodynamics*. Cambridge University Press.

[24] Abbott, I., and Von Doenhoff, A., 1960. *Theory of Wing Sections*. Dover Publications Inc.

[25] Jones, D., Schonlau, M., and Welch, W., 1998. "Efficient global optimization of expensive black-box functions". *Journal of Global Optimization,* ***13***(4), pp. 455–492.

[26] Sederberg, T., and Parry, S., 1986. "Free-form deformation of solid geometric models". In SIGGRAPH '86 Dallas, August 18-22, Vol. 20.

[27] Huyse, L., Padula, S., Lewis, R., and W., L., 2002. "Probabilistic approach to free-form airfoil shape optimization under uncertainty". *AIAA Journal,* ***40***(9), pp. 1764–1772.

[28] Widhalm, M., Ronzheimer, A., and Hepperle, M., 2007. "Comparison between gradient-free and adjoint based aerodynamic optimisation of a flying wing transport aircraft in preliminary design". In 25th AIAA Applied Aerodynamics Conference, Miami, FL.

[29] Lassila, T., and Gianluigi, R., 2010. "Parametric free-form shape design with pde models and reduced basis method". *Computer Methods in Applied Mechanics and Engineering,* ***199***(23-24), pp. 1583–1592.

[30] Jones, D., 2001. "A taxonomy of global optimization meth-

ods based on response surfaces". *Journal of Global Optimization,* ***21***(4), pp. 345–383.

[31] Armstrong, I., and Edmunds, T., 1989. "Fully automatic analysis in the industrial environment". In Proceedings of Second International Conference on Quality Assurance in Finite Element Analysis, NAFEMS.

[32] Edmunds, T., 1993. "Practical three dimensional adaptive analysis". In Proceedings of the Fourth International Conference on Quality Assurance and Standards, NATEMS.

[33] Forrester, A., Bressloff, N., and Keane, A., 2006. "Optimization using surrogate models and partially converged computational fluid dynamics simulations". *Proceedings of the Royal Society A,* ***462***(2071), pp. 2177–2204.